Nanoscale

Controllable Synthesis of Environmentally Stable vdW Antiferromagnetic Oxyhalide CrOCl

Journal:	*Nanoscale*
Manuscript ID	NR-ART-09-2024-003715.R1
Article Type:	Paper
Date Submitted by the Author:	10-Dec-2024

Complete List of Authors:	Banerjee, Rounak; Arizona State University The College of Liberal Arts and Sciences, Department of Physics Uppala, Sai; Arizona State University Ira A Fulton Schools of Engineering, Materials Science and Engineering Kopaczek, Jan; Wroclaw Univesity of Technology, Faculty of Fundamental Problems of Technology Ahmed, Sakib; Arizona State University Ira A Fulton Schools of Engineering, School of Electrical, Computer and Energy Engineering Wu, Cheng Lun; Arizona State University Ira A Fulton Schools of Engineering Kumar, Mukesh; Arizona State University Ira A Fulton Schools of Engineering Yumigeta, Kentaro; Arizona State University Celano, Umberto; Imec, Materials and Components Analysis; Arizona State University Ira A Fulton Schools of Engineering, School of Electrical, Computer and Energy Engineering Tongay, Seth Ariel; Arizona State University Ira A Fulton Schools of Engineering, Materials Science and Engineering

SCHOLARONE™
Manuscripts

Controllable Synthesis of Environmentally Stable vdW Antiferromagnetic Oxyhalide CrOCl

Rounak Banerjee[1,2,#] Sai Uppala[1,#] , Jan Kopaczek[1,3], Sakib Ahmed[4], Cheng-Lun Wu[1], Mukesh Kumar[1], Kentaro Yumigeta[1,5], Umberto Celano[4] and Seth Ariel Tongay[1,*]

[1]Materials Science and Engineering, School for Engineering of Matter, Transport and Energy, Arizona State University, Tempe, AZ 85287, USA

[2]Department of Physics, College of Liberal Arts and Sciences, Arizona State University, Tempe, AZ 85287, USA

[3]Department of Semiconductor Materials Engineering, Faculty of Fundamental Problems of Technology, Wroclaw University of Science and Technology, Wybrzeże Wyspiańskiego 27, Wrocław, 50–370 Poland

[4]School of Electrical, Computer and Energy Engineering, Arizona State University, Tempe, AZ 85287, USA

[5]Materials Science and Engineering Department, University of Arizona, Tucson, AZ, USA

[#] These authors contributed equally to this work.

*Corresponding author: stongay@asu.edu

Abstract

Layered antiferromagnetic oxyhalides with high environmental stability have recently attracted significant interest owing to their applications in spintronics and quantum devices. These materials can sustain a host of interesting phenomena that arise from magnetic phase transitions associated with structural changes. Although bulk crystal synthesis for some members of this oxyhalide family has been previously reported, bottom-up approaches for scalable growth remain limited. In this work, we demonstrated the controllable synthesis of CrOCl on different substrates through atmospheric pressure chemical vapor deposition (APCVD) technique using $CrCl_3$ and $KMnO_4$ precursors. Our results demonstrate the successful gas-phase reaction and subsequent nucleation followed by island growth on different target substrates. Comprehensive structural and optical characterization reveals that the effect of temperature, growth time, and carrier gas flow rates ultimately dictate the overall phase and morphology of the crystal. Overall, our findings enhance the understanding of the bottom-up growth mechanisms for synthesizing layered oxyhalides and further expand the library of stable magnetic oxides.

Keywords: Oxyhalides, layered antiferromagnet, magnetic oxides, chemical vapor deposition, CrOCl, angle-resolved Raman spectra, CVD

Introduction

Two-dimensional (2D) materials[1] have been extensively studied over the past two decades owing to their unique properties arising from size/quantum confinement effects[2] and symmetry breaking. Prior studies[3] have shown that completely new material properties arise as the dimensionality is reduced from 3D to 2D. Examples include room temperature excitons[4], valleytronic response[5], strongly anisotropic behavior in quasi-2D systems[6], enhanced superconductivity[7], topology[8], and Moire lattice-induced exotic properties[9]. In the search for magnetic analogs of 2D metals, semiconductors, and insulators, early studies focused on magnetic ordering in Fe_3GeTe_2[10], CrI_3[11], and $FePS_3$[12] material systems. However, these early examples of 2D magnets, along with other popular dihalide and trihalide systems, show high sensitivity to oxidization and environmental degradation effects, often taking minutes to days, creating immense difficulties in their characterization and eventual transition to realistic civilian applications.

Recent studies[13-20] have shown that 2D van-der Waals (vdW) transition metal oxyhalides are anisotropic layered magnets[13] with exceptional ambient stability while possessing unique properties arising from its temperature-dependent structural and magnetic phase transition[17]. These oxyhalide magnets have the general chemical formula MOX, where M stands for metals such as Sc, Ti, V, Cr, and Fe, while X is halide, Cl, or Br. Oxyhalides possess a Pmmn-type orthorhombic crystal structure with 2D sheets of CrOCl separated by weak vdW bonds, as depicted in Figure 1a,b. Studies show they are wide-gap semiconductors[13] with ~2.3 eV band gap and possess paramagnetic to antiferromagnetic ordering at around 13K[17]. They exhibit large optical anisotropy[21], and their strong antiferromagnetism[19,13] coupled with their weak interlayer bonding[22] and high environmental stability[13] makes them an ideal testbed system to optically engineer their magnetic properties. However, despite their attractive magnetic properties and outstanding environmental stability, fundamental studies to realize their bottom-up synthesis remain at seminal stages due to difficulties with complex precursor chemistry and co-existing phases with different stoichiometry in their phase diagram.

In this work, we demonstrate the first synthesis of environmentally stable ultra-thin sheets of vdW magnetic CrOCl using Atmospheric-Pressure Chemical Vapor Deposition (APCVD) technique. The technique relies on using relatively high vapor pressure $CrCl_3$ and $KMnO_4$ precursors and the high-temperature gas-phase reaction between the oxygen molecules supplied by $KMnO_4$ and the volatile $CrCl_3$ vapor, to realize CrOCl sheets on the Mica or sapphire surfaces. The quality of the resultant CrOCl sheets strongly depends on the concentration of the oxygen radicals controlled by the position of the $KMnO_4$ precursor, while the substrate temperature controls the nucleation density. Our systematic growth studies show that morphology and the phase of the material are strongly affected by various factors, such as the carrier gas flow rate, the growth time, and the growth temperature. Comprehensive characterization tools confirm the stoichiometry and crystallinity of the CVD-grown CrOCl sheets, while microscopy and spectroscopy techniques establish the commonly observed growth modes and morphology. The overall results introduce the required precursor chemistry and foundations for the first demonstration of APCVD of these highly stable CrOCl oxyhalide magnets.

Results and Discussions

I. Precursor chemistry and growth system design

Ultra-thin sheets of CrOCl have been synthesized via APCVD in an inert Argon (Ar) environment using a horizontal research-grade CVD tube furnace, as depicted in Figure 1c and SI Figure S1. Here, APCVD was selected owing to their cost-effectiveness for producing research-grade CrOCl while offering easy control over synthesis parameters, lab-grade scalability, and flexibility in substrate selection. Typical growths contain 40 mg of crushed ultrapure CrCl3 powder (Sigma Alrich, 99.5%) mixed with transport promoter (~9 mg) NaCl (Sigma Aldrich, >99%) placed in a ceramic boat at the center zone of the tube furnace (Lindberg Blue, M). The center zone is kept at 700-800 °C, though 750 °C yields optimal results to achieve sufficient vapor pressure of the non-volatile precursors. $KMnO_4$ (Sigma Aldrich, >99%) is placed upstream at the lower temperature zone (200-220 °C) due to its volatile nature. Here, $KMnO_4$ is selected to offer sufficient oxygen to stabilize CrOCl sheets since other Cr-based oxygen precursors, such as Cr_2O_3, require much higher growth temperatures, readily stabilizing other Cr complexes instead of CrOCl. The growth substrates were placed downstream from the $CrCl_3$ precursor (~6-10 cm), and the substrate temperature was kept at the 630-700 °C range to stabilize CrOCl sheets. Since popular substrates, such as Si/SiO_2, InP, and GaAs, decompose at the temperatures required to realize CrOCl, mica and sapphire were chosen as target substrates owing to their high thermal stability, with their oxide surfaces enhancing the surface nucleation of CrOCl precursors. The exact temperature range for the precursors, as well as the substrates, are depicted in Figure 1d. Prior to growth, the tube was evacuated to a base pressure of 10^{-2} torr and then

backfilled with Ar (purity> 99.5%) gas to ambient pressure. Ar flow rate was then maintained at 500 sccm while the system was purged for 10 minutes to avoid contamination from any residual gases. Finally, the Ar carrier gas flow rate was adjusted to 12.5 sccm and the furnace temperature was ramped up from ambient to 750 °C at 30 °C/min. The temperature was maintained for 40 minutes for optimum growth, after which the furnace was allowed to naturally cool to ambient temperature. Large area growth of thin sheets of CrOCl was obtained on the target substrate, as shown in Figure 1e.

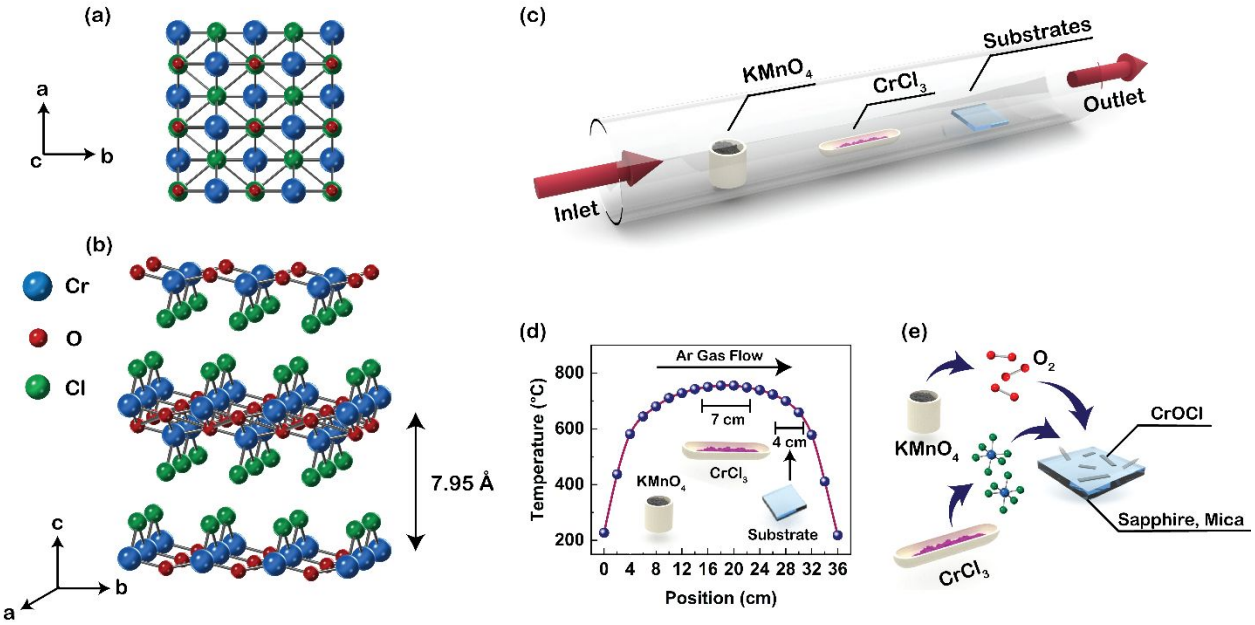

Figure 1: Crystal Structure and CVD set-up of CrOCl (a) Top-view (along c-axis) and (b) side-view of CrOCl crystal structure (c) Schematic diagram of CVD set-up depicting the relative positions of the precursors and target substrates (d) Temperature profile of the furnace depicting relative temperature ranges for the precursors and substrates (e) Schematic description of thin flake formation via APCVD.

II. Optical and Structural characteristics of CrOCl layers grown by APCVD

Figure 2a shows the low-magnification optical image of a typical CVD growth of CrOCl on a *c*-cut sapphire substrate. High-resolution Wavelength Dispersive Spectroscopy (WDS) performed on selected CVD-grown sheets (both large-area scans and single sheets) reveal elemental uniformity across the sheets, as evidenced by the WDS maps shown in Figure 2b-g. Confirmation of stoichiometry is obtained through both WDS and XPS (SI Figure S2). Raman spectroscopy measurements on as-synthesized CrOCl (Figure 2h) show three prominent out-of-plane peaks, namely A^1_g, A^2_g, and A^3_g, at 209 cm^{-1}, 416 cm^{-1} and 456 cm^{-1}, respectively, which aligns well with the literature. The corresponding Raman maps for these three modes are shown in SI Figure S3. We note that the A^2_g mode partially overlaps with Raman modes for the sapphire substrate. Thus, A^1_g and A^3_g peaks offer a better measure of the crystalline properties of CrOCl when deposited on sapphire substrates. The FWHM of these Raman peaks measures 6.45 cm^{-1}, 6.7 cm^{-1}, and 9.0 cm^{-1}, respectively, highlighting the quality of the synthesized sheets. Notably, the CrOCl sheets only appear when the growth temperature is 700 - 750 °C for both mica and sapphire substrates, as shown in Figure 2i, j. As the growth temperature is raised from 750 to 850 °C, triangular and hexagonal[23] Cr_2O_3 sheets appear (Figure 2k) accompanied by the broad A_g peak[24] at about 560 cm^{-1} in Figure 2h. Here, the observed triangular and hexagonal terminations in Cr2O3 likely arise from growth rate variations among crystal faces, influenced by surface and edge energy.

The growth occurs over large areas across the sapphire substrates (Figure 2a), with the nucleation density remaining high; however, these grown CrOCl sheets do not coalesce to form full area coverage. This suggests that the lateral growth speed of these CrOCl sheets is low. Microscale spatial resolution XRD datasets on both sapphire and mica show CrOCl sheets are highly crystalline and display strong (00l) reflections positioned at 2θ = 11.4°, 34.7°, 47.1°, 59.7° which agree well with literature[13] (Figure 3a, b). The surface morphology of the CVD-grown CrOCl sheets exhibit smooth surfaces, as shown in the Atomic Force Microscopy surface scans in Figure 3c, d. We also note that the typical CrOCl flake thickness ranges from 5-100 nm in thickness, which means the out-of-plane growth (Frank van der Merwe mode) is favorable without the formation of nanoclusters.

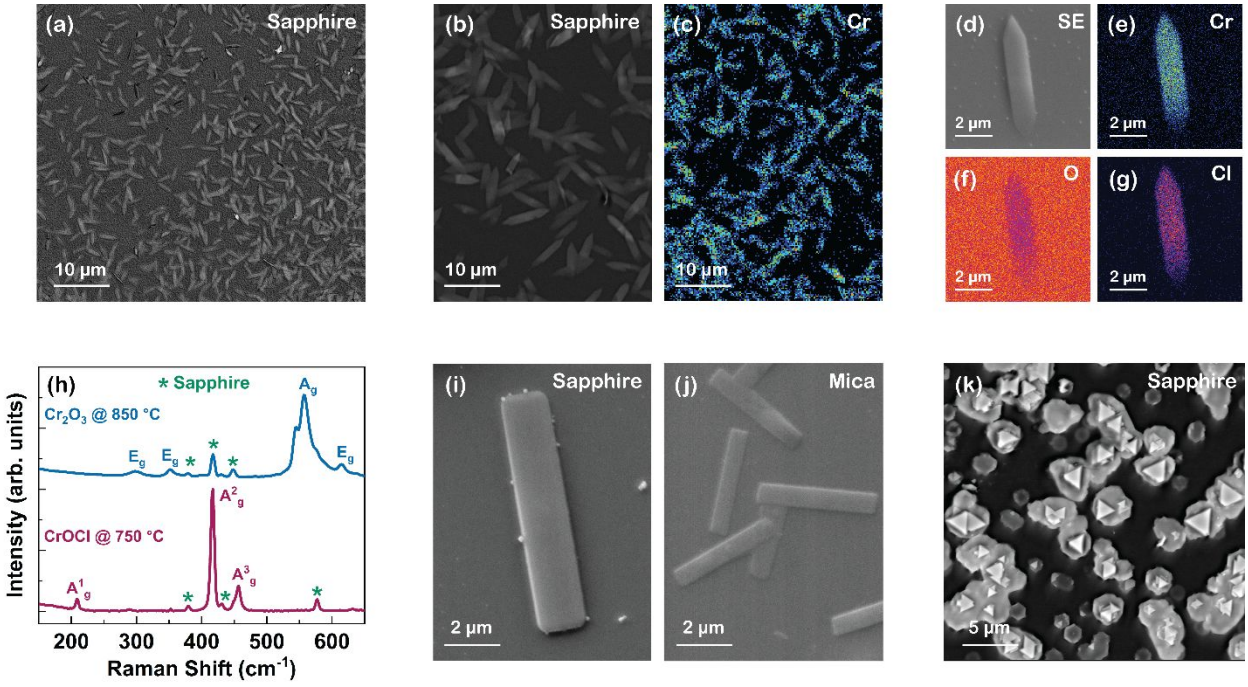

Figure 2: Optical Characterization of CrOCl Sheets (a) Confocal optical image of CVD-grown CrOCl on sapphire (b-c) Low magnification Secondary Electron (SE) image and corresponding Wavelength-Dispersive Spectroscopy (WDS) map showing uniformity across multiple CrOCl sheets (d-g) Elemental WDS maps for a single CVD grown CrOCl sheet on sapphire (h) Raman spectrum of CrOCl sheets on sapphire substrates with growth temperature of 750 °C and 850 °C (i-j) High magnification SE images showing rectangular planar CrOCl sheets on Sapphire and Mica substrates (k) Backscattered Electron (BSE) image of CVD grown triangles and hexagons of Cr_2O_3, at high growth temperature (~850 °C) on sapphire.

The growth mechanism in sapphire with triangular-edged layers growing on top of each other is clearly visible in Figure 3c. However, not all sheets have similar growth mechanisms, suggesting that further studies are needed to comprehensively understand the growth modes for different substrates.

Our findings suggest that the precursors undergo a solid-to-vapor transformation followed by a gas phase decomposition into their constituent species to yield CrOCl layers. The decomposition reaction of CrCl3 represents a complex behavior where congruent sublimation and incongruent decomposition happen simultaneously. The possible reaction steps are outlined below.

$$2\,KMnO_4(s) \leftrightarrow MnO_2(g) + K_2MnO_4(g) + O_2(g) \qquad \text{(Step 1.1)}$$

$$CrCl_3(s) \leftrightarrow CrCl_3(g) \qquad \text{(Step 1.2)}$$

$$CrCl_3(s) \leftrightarrow CrCl_2(s) + \frac{1}{2}Cl_2\ (g) \quad \text{(Step 1.3)}$$

$$CrCl_3(s) + \frac{1}{2}\,Cl_2\ (g) \leftrightarrow CrCl_4(g) \quad \text{(Step 1.4)}$$

$$2\ CrCl_4(g) + O_2(g) \leftrightarrow 2\ CrOCl\ (s) + 3\ Cl_2\ (g) \quad \text{(Step 2)}$$

$$2\ CrCl_3(g) + O_2(g) \leftrightarrow 2\ CrOCl\ (s) + 2\ Cl_2\ (g) \quad \text{(Step 3)}$$

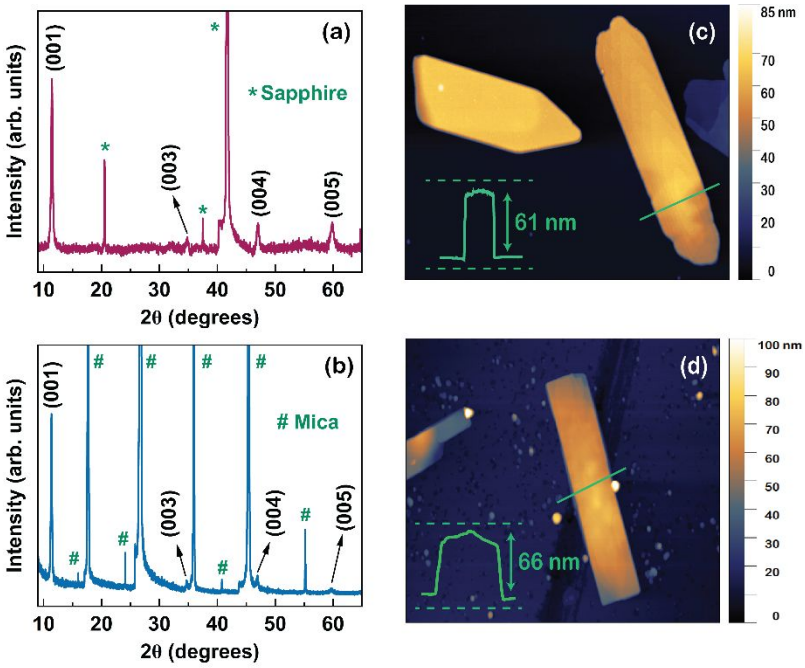

Figure 3: Structural and Morphological Characterization of CrOCl sheets (a-b) X-Ray Diffraction of planar sheets with large area coverage on sapphire and Mica substrates (c) Morphology of CVD grown thick sheets on Sapphire and (d) Mica depicting the layer-by-layer growth mechanism in CrOCl sheets

In step 1.1, the KMnO4 (s) decomposes into MnO2 and K2MnO4 along with O2 gas as a byproduct. In parallel, stable CrCl3 (s) sublimes into CrCl3 vapor (step 1.2), and simultaneously, it forms CrCl4 vapor (step 1.4). These reactive intermediate species are then transported downstream by the Ar carrier gas, where they adsorb onto the substrate. In the absence of sufficient O2, CrCl3 (precursor) growth is instead promoted on the substrate, as shown in SI Figure S4.

The reactive oxygen species from the decomposition of KMnO4 reacts with the CrCl3 and CrCl4 vapor on sapphire and mica substrates within the boundary layer and nucleates on the substrate surface to form CrOCl. These nucleation spots can be seen on sapphire substrates in Figure 2d. We note that while reacting byproduct O2 with CrCl4 (g) is essential to yielding CrOCl, passing O2 carrier gas in parallel with step 1.4 is not sufficient to deposit CrOCl, and thus step 1.1 is critical to the successful deposition of CrOCl. This can be attributed to the oxidization of CrCl3 precursors in the presence of flowing O2 gas instead of the transition from CrCl3 to volatile CrCl4 with inert Ar gas flow. With this picture in mind, step 1.1 serves as a controllable source of O2 (g), while step 1.4 provides the reactive CrCl4 gas to react with the byproduct O2 on the sapphire surface. Following step 1.2, steps 1.4 through 3 depict the two possible growth pathways to realize CrOCl sheets, with both CrCl4 and CrCl3 reacting with O2 to form the final product.

Previously, angle-resolved Raman spectroscopy was utilized to probe the structural crystallinity/anisotropy as well as the degree of structural anisotropy in other vdW systems such as ReS_2[6], GaTe[25], TiS_3[26], and

others[27,28]. Angle-resolved Raman measurements are performed on the CVD-grown sheets to determine the crystalline anisotropy. Figure 4a-c shows the polar plots from the angle-resolved Raman spectrum of a typical flake

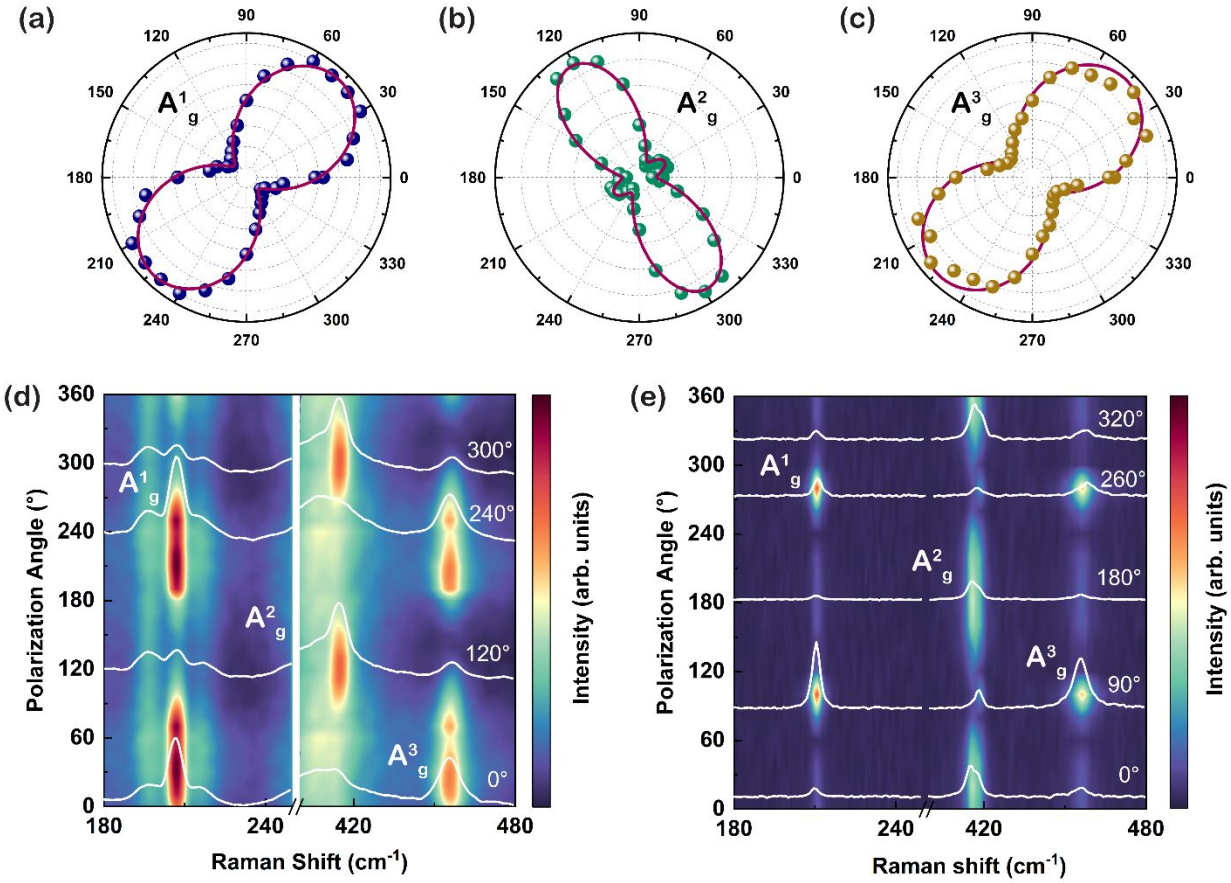

Figure 4: Polarized Raman Spectroscopy of CVD-grown flake on Mica and Sapphire. (a-c) Polar plots for the three Raman modes under parallel laser polarization (d-e) Contour color map of A^1_g, A^2_g, and A^3_g modes for mica and sapphire substrates, respectively. The orientation of the flake is shown in SI Figure S5.

deposited on mica with laser polarization oriented parallel to the *a*-axis of the crystal. Angle-resolved measurements show that the relative Raman peak intensities dramatically change as the polarization vector of the incoming laser source varies. These changes are better captured in contour color maps for mica and sapphire substrates, as shown in Figure 4d-e when the laser polarization angle was changed from 0 to 360° with a step size of 10°. As seen from Fig 4a-c, all the prominent modes show a two-fold symmetry consistent with existing literature[21], with maxima occurring along the a-axis direction, while minima occur in the perpendicular orientation. Furthermore, the A^1_g and A^3_g modes maximize at 30° and 210°. In comparison, the A^2_g mode maximizes at 120° and 300°, suggesting that electron-photon interaction for this mode is dominant in a perpendicular direction from the other modes.

III. Factors influencing the overall growth characteristics

The quality of the CVD-grown sheets depends on several factors, including the quantity of precursor material (which determines the concentration of reactive species O_2 and $CrCl_2$), substrate temperature, and growth time. In addition to these, the results show that the Argon carrier gas flow rates have a direct influence on the overall coverage, while the growth time directly influences the morphology of the CVD-grown CrOCl

sheets. Here, the flow rate determines how fast the precursor vapors are transported to the substrate and directly influences the boundary layer profile at the substrate-vapor interface, which in turn influences the diffusion, chemisorption, and subsequent nucleation processes on the substrate surface. These effects are clearly captured by a series of scanning electron microscopy (SEM) images in Figure 5a-f and SI Figure S6. As

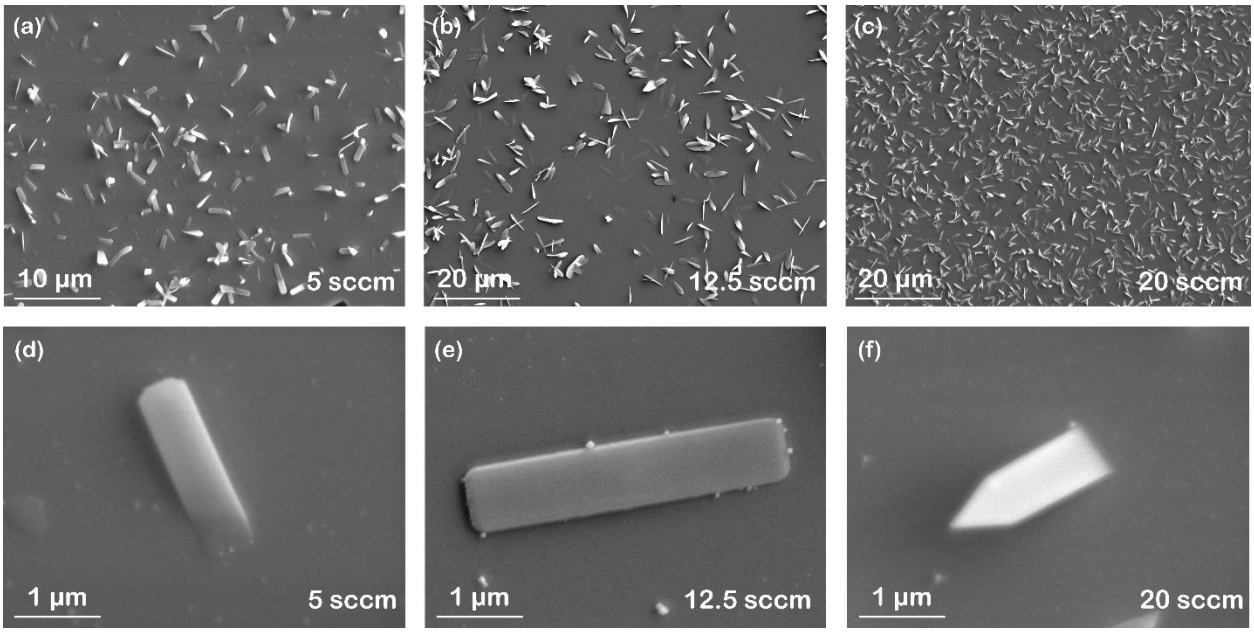

Figure 5: Effect of carrier gas flow rate on the morphology of CVD-grown sheets on sapphire substrates (a-c) Low magnification SE images at different flow rates (d-f) Selected area high magnification SE images showing the different morphologies of CVD grown sheets

the flow rate is increased from 5 sccm to 20 sccm at optimal growth temperature (750 °C) and a growth time of 40 minutes, the growth coverage increases as the reactant precursor vapors are more efficiently transported to the surface with thinner boundary layer. Interestingly, the morphology of the CrOCl grown sheets changes as the growth time is increased from 15 to 40 minutes (Figure 6a-f). Deposited CrOCl sheets have a triangular edge finish for shorter CVD growth times. These triangular edges (Figure 6d) change into more rectangular edges as the growth time is increased to 40 minutes (Figure 6f). The crossover between the triangular to rectangular edge finish can also be evidenced by more rounded features observed between 15-40mins (Figure 6e). This behavior, at first sight, can be attributed to different growth rates (kinetic rates) in particular crystalline directions. More specifically, CrOCl sheets first grow in the longitudinal direction after the initial nucleation process, but the longitudinal growth halts once these triangle tips are formed.

Additional growth time does not promote further longitudinal growth but terminates it at the sharp edge. The incoming precursors instead promote growth in different crystalline directions, as evidenced by Figure 6e, till they completely terminate the edges, as shown in Figure 6f. The nature of this termination process or the edge construction is not completely understood and warrants future studies.

It is also noteworthy that CrOCl sheets grow both in-plane (adhering to the sapphire substrate) and out-of-plane direction (from the substrate), as shown in Figure 5a-c, but more notably in Figure 6b. These out-of-plane grown CrOCl sheets abruptly nucleate on the sapphire substrate and grow in that crystalline registry in the out-of-plane direction, usually at acute (~30o) angles, as seen in SI Figure S7. This potentially suggests that the CrOCl and sapphire lattice mismatch is large and/or the surface energy of the sapphire substrate is lower than that of CrOCl sheets, and further substrate engineering studies are needed to understand the underlying reasons behind this in and out-of-plane growth characteristics. Initial studies on

mica substrates show that CrOCl sheets have growth characteristics similar to those of sapphire (see SI Figure S6), while SiO_2 and Si do not promote CrOCl growth. Furthermore, low-pressure (LPCVD) processes result in large area coverage due to the larger mean free path of the reactant species, but they also result in a loss of rectangular morphology, as seen in SI Figure S8.

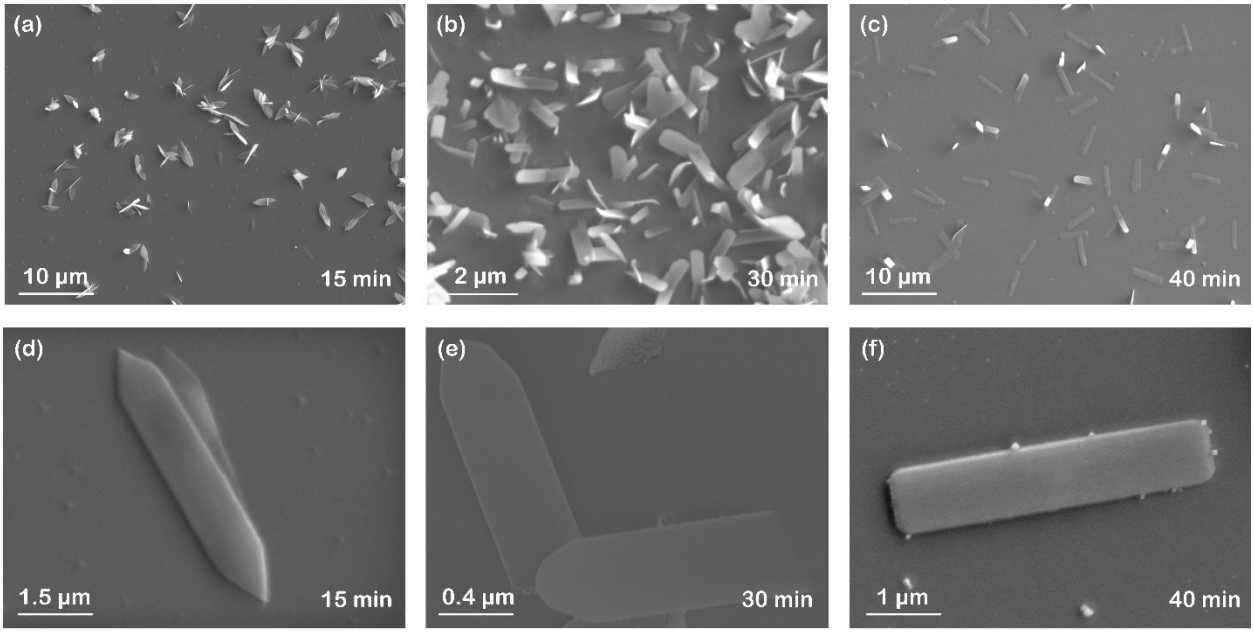

Figure 6: Effect of growth time on the morphology of CVD-grown sheets on sapphire substrates (a-c) Low magnification SE images at different growth times (d-f) High magnification SE images highlighting the gradual change in morphology as the growth time is increased.

Conclusions

In summary, the work introduced the first APCVD growth of environmentally stable 2D oxyhalide magnet CrOCl growth using $CrCl_3$ and $KMnO_4$ precursors in the presence of argon carrier gas. The results introduced chemical reaction steps to realize CrOCl sheets, starting with the precursors as mentioned above. Comprehensive characterization studies have shown that the deposited CrOCl exhibits high structural quality, as evidenced by various metrology tools. CrOCl sheets do not contain any Cr_2O_3 phases, and their surfaces remain unoxidized. While the CVD growth of CrOCl growth is feasible with the suggested growth route, deposited CrOCl sheets still do not coalesce, possibly due to the unique kinetic rate halting edge termination, and thus remain isolated without reaching a full coverage. With the CrOCl growth routes introduced in this work and the successful demonstration of environmentally stable magnetic oxyhalide CrOCl growth, future studies are needed to engineer the substrate type further – well beyond sapphire, mica, Si, and SiO_2/Si to understand the role of substrates on in-plane *vs.* out-of-plane growth dynamics as well as to achieve large scale fully merged CrOCl sheets.

Methods

Substrate preparation for CVD growth: To facilitate the growth of CrOCl, c-cut sapphire wafers 2 inches in diameter were sectioned into 1 cm x 2 cm substrates using a diamond pen. Prior to growth, the substrates underwent extensive cleaning to remove surface contamination. Initially, the substrates were treated with piranha solution, composed of 30 ml of H_2SO_4 mixed with 10 ml of H_2O_2 in a beaker. After thorough mixing, the substrates were immersed in the solution and removed after 15 -20 minutes, allowing it to reach ambient

temperature. Subsequently, the substrates underwent additional cleaning involving immersion in deionized (DI) water, ethanol, and isopropyl alcohol (IPA). Each cleaning step was conducted for 10 minutes in an ultrasonication chamber to ensure the complete removal of any remaining residues of the piranha solution. Following this, O_2 plasma cleaning for 15 minutes at 25 mW was conducted to remove surface contamination further. Cleaving was achieved using a razor blade for mica substrates, followed by a similar 15-minute oxygen plasma treatment.

Wavelength-Dispersive Spectroscopy: A JEOL JXA 8530-F Field-Electron Electron-Probe Microanalyzer (EPMA) with a sub-micron spot size was used to perform high-resolution Wavelength-Dispersive Spectroscopy (WDS). An acceleration voltage of 15kV coupled with a beam current of 50nA was used to confirm crystal stoichiometry. Secondary-Electron (SE) images were taken at 15kV with a beam current of 15 nA.

Atomic Force Microscopy: Sample morphology was studied using an NT-MDT SPECTRA modular AFM. A Bruker RESPA probe with a resonance frequency of 40 kHz and spring constant ~5 N/m was used for scanning in semi-contact and contact mode. All images underwent processing in Gwyddion software.

X-Ray Diffraction: A Rigaku Smart Lab HRXRD system was used to measure the X-ray diffraction of the sheets on a sapphire substrate. Cu Kα radiation with λ=1.54186 Å was used to scan in θ/2θ mode from 5° to 70° with a step size of 0.01° at 40kV and 44mA. A length-limiting slit of 0.5 mm was used to further collimate the beam to a Hypix-3000 detector.

Raman Spectroscopy: A Renishaw inVia Raman spectrometer with a backscattering configuration was used to collect Raman spectrum with λ_{ex}~488 nm. The laser power was fixed at 2 mW to minimize sample degradation. 10 s of exposure time and 3 accumulations were typically used for collecting data. The signal was collected with a 100x objective after being dispersed by 2400 lines/mm grating. Angle-resolved Raman measurements were performed on a custom-built micro-Raman setup with a 532 nm laser in a backscattering configuration. The scattered signal was dispersed using a 1200 lines/mm grating, and a thermoelectrically cooled Andor detector was used to collect the signal. A 100X Mitutoyo objective lens focused the laser, and the spot size was confined to ~1 μm. The laser power was set at 12 mW to achieve a good signal-to-noise ratio from the small sheets.

X-Ray Photoelectron Spectroscopy: X-ray photoelectron spectroscopy (XPS) was conducted using an Axis Supra+ instrument from Kratos Analytical. Al Kα radiation at 1486.6 eV was used for this measurement with an emission current of 20 mA.

Author Contributions

Rounak Banerjee: Formal analysis (lead), Investigation (lead), Validation (lead), Visualization (lead), Writing - original draft (lead), Writing - review and editing (lead)
Sai Uppala: Formal analysis (supporting), Investigation (supporting), Validation (supporting),
Jan Kopaczek: Writing-original draft (supporting), Writing-review and editing (supporting)
Sakib Ahmed: Investigation (supporting)
Cheng-Lun Wu: Investigation (supporting)
Mukesh Kumar: Investigation (supporting)

Kentaro Yumigeta: Visualization (supporting)
Umberto Celano: Writing - review and editing (supporting)
Seth Ariel Tongay: Conceptualization (lead), Funding acquisition (lead), Supervision (lead), Writing - original draft (lead), Writing – review and editing (lead)

Conflict of Interest. The authors have no conflicts of interest to disclose.

Acknowledgments. S.T. acknowledges primary support from DOE-SC0020653 (materials synthesis), NSF ECCS 2052527 for initial spectroscopy tests, DMR 2111812 for phononic characterization, NSF CBET 2206987 for precursor design, CMMI 2129412 for manufacturing platforms, NSF CMMI 1825594 for NMR and TEM studies, NSF DMR-1955889 for magnetic measurements) Lawrence Semiconductors for generous support for a student and Applied Materials Inc. The use of facilities within the Eyring Materials Center at Arizona State University is partly supported by NNCI-ECCS-1542160.

References

(1) Mannix AJ, Kiraly B, Hersam MC, Guisinger NP. Synthesis and chemistry of elemental 2D materials. Nat Rev Chem. 2017;1(2). http://dx.doi.org/10.1038/s41570-016-0014

(2) Liu X, Hersam MC. 2D materials for quantum information science. Nat Rev Mater . 2019;4(10):669–84. http://dx.doi.org/10.1038/s41578-019-0136-x

(3) Li W, Qian X, Li J. Phase transitions in 2D materials. Nat Rev Mater . 2021;6(9):829–46. http://dx.doi.org/10.1038/s41578-021-00304-0

(4) Calman EV, Fogler MM, Butov LV, Hu S, Mishchenko A, Geim AK. Indirect excitons in van der Waals heterostructures at room temperature. Nat Commun . 2018;9(1). http://dx.doi.org/10.1038/s41467-018-04293-7

(5) Schaibley JR, Yu H, Clark G, Rivera P, Ross JS, Seyler KL, et al. Valleytronics in 2D materials. Nat Rev Mater . 2016;1(11). http://dx.doi.org/10.1038/natrevmats.2016.55

(6) Chenet DA, Aslan B, Huang PY, Fan C, van der Zande AM, Heinz TF, et al. In-plane anisotropy in mono- and few-layer ReS2 probed by Raman spectroscopy and scanning transmission electron microscopy. Nano Lett . 2015;15(9):5667–72. http://dx.doi.org/10.1021/acs.nanolett.5b00910

(7) Navarro-Moratalla E, Island JO, Mañas-Valero S, Pinilla-Cienfuegos E, Castellanos-Gomez A, Quereda J, et al. Enhanced superconductivity in atomically thin TaS2. Nat Commun . 2016;7(1). http://dx.doi.org/10.1038/ncomms11043

(8) Sulaev A, Zeng M, Shen S-Q, Cho SK, Zhu WG, Feng YP, et al. Electrically tunable in-plane anisotropic magnetoresistance in topological insulator BiSbTeSe2 nanodevices. Nano Lett . 2015;15(3):2061–6. http://dx.doi.org/10.1021/nl504956s

(9) He F, Zhou Y, Ye Z, Cho S-H, Jeong J, Meng X, et al. Moiré patterns in 2D materials: A review. ACS Nano. 2021;15(4):5944–58.

http://dx.doi.org/10.1021/acsnano.0c10435

(10)Fei Z, Huang B, Malinowski P, Wang W, Song T, Sanchez J, et al. Two-dimensional itinerant ferromagnetism in atomically thin Fe3GeTe2. Nat Mater . 2018;17(9):778–82. http://dx.doi.org/10.1038/s41563-018-0149-7

(11)Jiang S, Li L, Wang Z, Mak KF, Shan J. Controlling magnetism in 2D CrI3 by electrostatic doping. Nat Nanotechnol . 2018;13(7):549–53. http://dx.doi.org/10.1038/s41565-018-0135-x

(12)Nauman M, Kiem DH, Lee S, Son S, Park J-G, Kang W, et al. Complete mapping of magnetic anisotropy for prototype Ising van der Waals FePS3. 2d Mater . 2021;8(3):035011. http://dx.doi.org/10.1088/2053-1583/abeed3

(13)Zhang T, Wang Y, Li H, Zhong F, Shi J, Wu M, et al. Magnetism and optical anisotropy in van der Waals antiferromagnetic insulator CrOCl. ACS Nano . 2019;13(10):11353–62. http://dx.doi.org/10.1021/acsnano.9b04726

(14)Ahn EC. 2D materials for spintronic devices. Npj 2D Mater Appl . 2020;4(1). http://dx.doi.org/10.1038/s41699-020-0152-0

(15)Iqbal MZ. Spin-valve effect of 2D-materials based magnetic junctions. In: Spintronic 2D Materials. Elsevier; 2020. p. 253–72. https://doi.org/10.1016/b978-0-08-102154-5.00009-6

(16)Miao N, Xu B, Zhu L, Zhou J, Sun Z. 2D Intrinsic Ferromagnets from van der Waals Antiferromagnets. J Am Chem Soc . 2018;140(7):2417–20. http://dx.doi.org/10.1021/jacs.7b12976

(17)Yang L, Gong Y, Lv Y, Huang S, Huang P, Huo D. Magnetic and thermodynamic study of the interplay between magnetism and structure in CrOCl. J Alloys Compd . 2024;982(173845):173845. http://dx.doi.org/10.1016/j.jallcom.2024.173845

(18)Wang R, Cui Q, Zhu W, Niu Y, Liu Z, Zhang L, et al. In-plane optical anisotropy of two-dimensional VOCl single crystal with weak interlayer interaction. Chin Physics B . 2022;31(9):096802. http://dx.doi.org/10.1088/1674-1056/ac7555

(19)Christensen AN, Johansson T, Quézel S. Preparation and magnetic properties of CrOCl. Acta Chem Scand . 1974;28a:1171–4. http://dx.doi.org/10.3891/acta.chem.scand.28a-1171

(20)Qian Z, Song Z, Wu J, Wang D, Wen W, Wang X, et al. Chemical vapor deposition and Raman spectroscopy of two-dimensional antiferromagnetic FeOCl crystals. J Phys Chem C Nanomater Interfaces . 2023;127(14):6785–92. http://dx.doi.org/10.1021/acs.jpcc.3c00970

(21)Liu J, Zheng M, Zhang X, Liu X, Luo S, Lin M, et al. Abnormal linear dichroism in anisotropic van der Waals crystal CrOCl revealed by phase-dependent polarized Raman scattering. Adv Opt Mater . 2024;12(16). http://dx.doi.org/10.1002/adom.202303190

(22)You S, Guo X, Jiang J, Yang D, Li M, Ouyang F, et al. Temperature−Dependent Raman scattering investigation on vdW epitaxial PbI2/CrOCl heterostructure. Crystals (Basel) . 2023;13(1):104. http://dx.doi.org/10.3390/cryst13010104

(23)Hafeez M, Siddique Saleemi A, Ur Rehman S, Adrees M, Mehmood S, Mir IA, et al. CVD growth of layered Cr2O3 hexagonal flakes for optoelectronic applications. Appl Surf Sci . 2021;536(147713):147713. http://dx.doi.org/10.1016/j.apsusc.2020.147713

(24)Bhardwaj P, Singh J, Kumar R, Kumar D, Verma V, Kumar R. Oxygen defects induced tailored optical and magnetic properties of FexCr2−xO3 (0 ≤ x ≤ 0.1) nanoparticles. Appl Phys A Mater Sci Process . 2022;128(2). http://dx.doi.org/10.1007/s00339-021-05233-x

(25)Fonseca JJ, Tongay S, Topsakal M, Chew AR, Lin AJ, Ko C, et al. Bandgap restructuring of the layered semiconductor gallium Telluride in air. Adv Mater . 2016;28(30):6465–70. http://dx.doi.org/10.1002/adma.201601151

(26)Wu K, Torun E, Sahin H, Chen B, Fan X, Pant A, et al. Unusual lattice vibration characteristics in whiskers of the pseudo-one-dimensional titanium trisulfide TiS3. Nat Commun . 2016;7(1). http://dx.doi.org/10.1038/ncomms12952

(27)Wu K, Chen B, Yang S, Wang G, Kong W, Cai H, et al. Domain architectures and grain boundaries in chemical vapor deposited highly anisotropic ReS2 monolayer films. Nano Lett . 2016;16(9):5888–94. http://dx.doi.org/10.1021/acs.nanolett.6b02766

(28)Song Q, Pan X, Wang H, Zhang K, Tan Q, Li P, et al. The in-plane anisotropy of WTe2 investigated by angle-dependent and polarized Raman spectroscopy. Sci Rep . 2016;6(1). http://dx.doi.org/10.1038/srep29254

(29)Wang S, Rong Y, Fan Y, Pacios M, Bhaskaran H, He K, et al. Shape evolution of monolayer MoS2 crystals grown by chemical vapor deposition. Chem Mater . 2014;26(22):6371–9. http://dx.doi.org/10.1021/cm5025662

(30)Yang SY, Shim GW, Seo S-B, Choi S-Y. Effective shape-controlled growth of monolayer MoS2 flakes by powder-based chemical vapor deposition. Nano Res . 2017;10(1):255–62. http://dx.doi.org/10.1007/s12274-016-1284-6

(31)Zhang J, Wang F, Shenoy VB, Tang M, Lou J. Towards controlled synthesis of 2D crystals by chemical vapor deposition (CVD). Mater Today (Kidlington) . 2020;40:132–9. http://dx.doi.org/10.1016/j.mattod.2020.06.012

Data Availability Statement

The data supporting this article have been included as part of Supplementary Information.

Additional datasets are available upon request from the authors.